A novel marker enhancement filter (MEF) for fluoroscopic images

Olesya Peshko[1], Timothy N Davidson[1], Jan Modersitzki[2], Tamás Terlaky[3] and Douglas J Moseley[4]

[1] McMaster University, Hamilton, ON L8S 4K1, Canada
[2] University of Lübeck, Lübeck, 23562, Germany
[3] Lehigh University, Bethlehem, PA 18015, USA
[4] Princess Margaret Hospital, Toronto, ON M5G 2M9, Canada

E-mail: peshkoo@mcmaster.ca

Abstract. To enhance the measurements of radio-opaque cylindrical fiducial markers in low contrast x-ray and fluoroscopic images, a novel nonlinear marker enhancement filter (MEF) has been designed. It was primarily developed to assist in automatic initialization of a tracking procedure for intra-fraction organ motion analysis in fluoroscopic sequences. Conventional procedures were not able to provide sufficient improvement due to the complications of noise, small marker size, cylindrical shape and multiple orientations, intensity variations of the background, and the presence of overlaying anatomical measurements in this application. The proposed MEF design is based on the principles of linear scale space. It includes measures that assess the probability of each pixel to belong to a marker measurement, morphological operations, and a novel contrast enhancement function for standardization of the filter output. The MEF was tested on fluoroscopic images of two phantoms and three prostate patients, and was shown to perform better or comparable to the existing filters in terms of marker enhancement and background suppression, while performing significantly better in marker shape preservation.

1. Introduction

Image guidance with kilovoltage imaging units mounted on a linear accelerator has become a conventional clinical practice for radiation therapy [1]. One particular example is the monitoring of intrafraction organ motion using fluoroscopic image sequences, i.e., temporal sequences of 2D x-ray projection images acquired with the system in a fixed position. Often, radio-opaque fiducial markers are inserted prior to planning to improve the reliability of target localization for organs with limited x-ray contrast, such as the prostate [2]. In order to measure the intrafraction organ motion of prostate patients, we are designing a method for tracking of the fiducial markers in lateral fluoroscopic image sequences [3][4]. Automatic tracking requires reliable initialization, i.e, finding marker positions in the first frame of a sequence. That is challenging due to the low contrast, noise, and the small marker size. In our case, the markers are gold cylinders 3 mm long and 0.8 mm in diameter, which, with our current geometric setup in which the pixel size measures 0.2604 mm near the isocentre of the linear accelerator, makes them appear as approximately 12×3 pixel measurements in the fluoroscopic images.

Several approaches for marker enhancement and detection have been reported in the literature, such as morphological opening [5], template matching [6][7], and the marker extraction

kernel [8]. For the best results on cylindrical markers, these methods require the use of multiple templates or preliminary knowledge of marker orientations. To improve the detection outcome, they have to be combined with other procedures, such as the application of noise reduction filters [5][8] or edge enhancement [6], and intensity thresholding [6], for which the selection of parameters that will work well for different images may represent another challenge. Finally, the above mentioned methods tend to distort the marker shape, which is undesirable for our application, as the fluoroscopic images are to undergo registration [9] to the daily verification 3D cone-beam computed tomography (CBCT) image for reliable tracking initialization.

In this paper, we propose a novel marker enhancement filter (MEF) that can be used alone or as a preprocessing component in multi-stage methods for marker enhancement and detection. The MEF amplifies the markers, suppresses the background and anatomical features, and preserves marker shapes. The proposed filter is designed within the linear scale-space framework [10] that has found wide utilization in the enhancement of vessels and other line-like and blob features, e.g., [11][12], and in feature detection and image matching applications for computer vision [13]. Methods based on scale space are typically able to achieve global contrast for the sought-for features in the images by combining the assumptions about their size and shape with the local contrast analysis. The MEF includes an adaptation of the vessel enhancement approach proposed by Frangi et al. [11], morphological operations [14], and a novel contrast enhancement function that is able to operate successfully on a variety of images with different intensity characteristics. While Frangi's method was targeted at enhancement of the tubular structures, the markers we seek to amplify are quite different, which leads to a different filter design. The fluoroscopic images are subject to temporal filtering with a Dolph-Chebyshev filter [15] prior to the MEF application, which provided the best contrast-to-noise ratio among other methods that we tested on a phantom with moving markers [4].

2. Marker enhancement filter design

2.1. Scale-space analysis

In computer vision, there is an accepted perspective that features in the images only meaningfully exist over limited ranges of scales [10]. To perform an automatic image interpretation, a multi-scale representation was proposed [10] (and references therein), in which the original image $\mathcal{A} : \mathbb{R}^2 \to \mathbb{R}$ is embedded into a one-parameter family of derived images $\mathcal{L} : \mathbb{R}^2 \times \mathbb{R}_+ \to \mathbb{R}$, where the additional non-negative scalar parameter is the scale. The scale-space representation is defined as the convolution of the image with the Gaussian functions of the appropriate scales:

$$\mathcal{L}(x, \sigma) = \mathcal{A}(x) * \mathcal{G}(x, \sigma) \text{ for } \sigma > 0, \text{ and } \mathcal{L}(x, 0) = \mathcal{A}(x), \tag{1}$$

where the Gaussian is defined as $\mathcal{G}(x, \sigma) = \exp\left(-\frac{\|x\|^2}{2\sigma^2}\right)/(2\pi\sigma^2)$, and $*$ denotes two-dimensional convolution. Due to the fact that the fiducial markers in our application are all of equal or very similar size to each other, we only compute $\mathcal{L}$ for one fixed scale, $\sigma = \sigma_0$, that is selected to amplify the features close in size to the markers.

A common approach to analyze the local behaviour of an image intensity function is to consider its second order Taylor expansion in the neighborhood of a point x_0 [11][12]. Some methods directly utilize second order derivatives of $\mathcal{L}$. For example, the Laplacian of Gaussian (LoG) [10] method was used in several studies for marker enhancement in portal images [16][17]. However, in addition to enhancing the markers, the LoG is prone to enhancing anatomical features that have a dimension that is of a similar scale to the markers. In the following sections we describe the proposed filter and show how it is able to overcome this issue.

2.2. MEF principles: Magnitude-and-ratio versus magnitude-only image

One way to characterize the contrast and shape of features in the image at a particular scale is to analyze the sign and magnitude of the eigenvalues of the Hessian matrix that is constructed

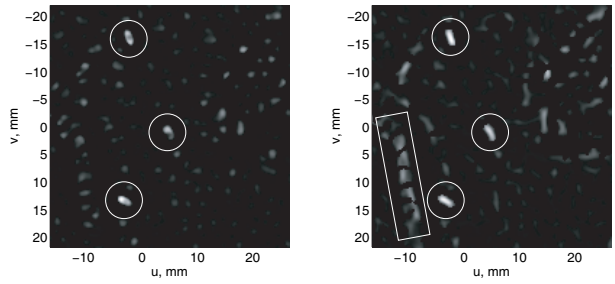

Figure 1. The magnitude-and-ratio $\mathcal{Y}_{\mathrm{mr}}$ (*left*) and magnitude-only $\mathcal{Y}_{\mathrm{m}}$ (*right*) images. While both attain high response in marker pixels (*encircled*), $\mathcal{Y}_{\mathrm{m}}$ is characterized with better marker shape preservation, but also undesirably amplifies long anatomical features (e.g., *in rectangle*).

from the second order derivatives of $\mathcal{L}$. For the bright markers on a dark background, the intensity function should: (i) be concave, which requires negative eigenvalues; (ii) possess a reasonable contrast that is reflected in the magnitude of the eigenvalues, and (iii) describe a feature whose dimensions are not very different, which can be assessed in terms of the ratio of the eigenvalues. To design a method for capturing these features, let λ_1 and λ_2 denote the eigenvalues of the Hessian of $\mathcal{L}(x, \sigma_0)$ at a given point $x = x_0$. The magnitude measure is defined as $\mathcal{X}_{\mathrm{m}} = \sqrt{\lambda_1^2 + \lambda_2^2}$, and the ratio as $\mathcal{X}_{\mathrm{r}} = \lambda_1/\lambda_2$, where $|\lambda_1| \leq |\lambda_2|$ [11]. An effective marker enhancement filter should provide high response in the image pixels with $\lambda_{1,2} < 0$, and large $\mathcal{X}_{\mathrm{m}}$ and $\mathcal{X}_{\mathrm{r}}$.

Based on the insight from the work of Frangi et al. [11], we incorporate $\mathcal{X}_{\mathrm{m}}$ and $\mathcal{X}_{\mathrm{r}}$ into probability-like measures, based on which we define a *magnitude-and-ratio image*:

$$\mathcal{Y}_{\mathrm{mr}} = \begin{cases} \left(1 - \exp\left(-\frac{\mathcal{X}_{\mathrm{m}}^2}{2\gamma^2}\right)\right)\left(1 - \exp\left(-\frac{\mathcal{X}_{\mathrm{r}}^2}{2\beta^2}\right)\right), & \text{if } \lambda_1 < 0 \text{ and } \lambda_2 < 0, \\ 0, & \text{otherwise,} \end{cases} \tag{2}$$

where γ and β are used to normalize the values of $\mathcal{X}_{\mathrm{m}}$ and $\mathcal{X}_{\mathrm{r}}$. As suggested in [11], γ is chosen to be half of the maximal $\mathcal{X}_{\mathrm{m}}$ value. For circularly shaped blobs, $\beta = 0.5$ would be used [11]. We reduce β to 0.25 based on visual observations of the filtered images in order to produce high response for a range of shapes from circular to elliptical blobs. Although the marker dimensions are known, it is not practical to tune the filter to elliptical blobs exclusively, as the measurements are often corrupted by the noise and overlaying structures, and rarely posses exactly the same ratio as the markers. Observing that the markers may often have reasonably high contrast in fluoroscopic images, we have also considered a *magnitude-only image*:

$$\mathcal{Y}_{\mathrm{m}} = \begin{cases} 1 - \exp\left(-\frac{\mathcal{X}_{\mathrm{m}}^2}{2\gamma^2}\right), & \text{if } \lambda_1 < 0 \text{ and } \lambda_2 < 0, \\ 0, & \text{otherwise.} \end{cases} \tag{3}$$

Comparing $\mathcal{Y}_{\mathrm{mr}}$ and $\mathcal{Y}_{\mathrm{m}}$ in application to our fluoroscopic images (see Figure 1), we notice that while the markers possess high intensities in both of them, $\mathcal{Y}_{\mathrm{m}}$ offers better marker shape preservation, but also undesirably amplifies long anatomical features similar in width to the marker size. To gain from the desirable properties of both images, we combine them by using $\mathcal{Y}_{\mathrm{mr}}$ as a mask for $\mathcal{Y}_{\mathrm{m}}$, i.e., the intensities in the filtered image are derived from $\mathcal{Y}_{\mathrm{m}}$, but only from the high-intensity regions of $\mathcal{Y}_{\mathrm{mr}}$.

2.3. Contrast enhancement function

Intensity thresholding is often used as a part of multi-stage procedures to improve the filtering outcome by further separating the sought-for markers from the background. It is typically

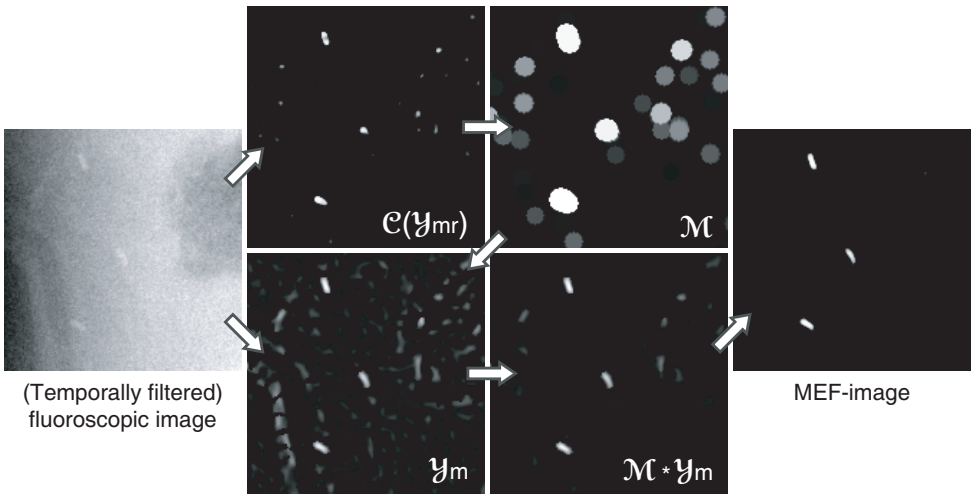

Figure 2. Steps of the MEF algorithm.

performed by setting all intensities in the image that fall below a preset value ϑ to the minimal background intensity, e.g., [6][17]. However, we prefer to use a smooth threshold function as it increases overall reliability of image registration that will be performed on the output of the MEF filter in the proposed application. In particular, given an image $\mathcal{Y}$ with values in $[0, 1]$ we will construct the contrast enhanced image $\mathcal{C}(\mathcal{Y}) = \mathcal{Y}^{\mathcal{Z}(\mathcal{Y})}$, where $\mathcal{Z}(\mathcal{Y}) = \frac{\vartheta^s \log_\vartheta \tau}{\vartheta^s - 1}\left(1 - \frac{1}{\mathcal{Y}^s}\right)$. In this expression ϑ is the threshold, τ is the minimum intensity of all marker points after contrast enhancement, and s is the sharpness of distinction between the marker and non-marker points. In our experiments we chose $\tau = 1/2$ and $s = 3$.

As in all thresholding methods, the choice of the ϑ is critical. For our application we have derived a marker-based model for choosing the threshold [4]: We seek to amplify as many bright pixels in the image, as there are expected to be occupied by the markers, and suppress everything else. For the cylindrical markers in the lateral images, where they appear full-length, the number of pixels can be approximated by $m = n\lceil 2rh/\delta^2 \rceil$, where n is the number of markers, r and h are their radius and length, respectively, and δ is the size of the pixel side. The intensity values in the image are sorted in a descending order, and the threshold ϑ is chosen to be the m-th element in this sorted sequence.

2.4. MEF algorithm

The MEF consists of the following steps, which are depicted in Figure 2:

- The scale-space representation is computed for a (temporally filtered) fluoroscopic image. We selected $\sigma_0 = 0.7$ mm for our application.
- Images $\mathcal{Y}_{\mathrm{m}}$ and $\mathcal{Y}_{\mathrm{mr}}$ are computed as described in Section 2.2, and $\mathcal{Y}_{\mathrm{mr}}$ is contrast enhanced by the function $\mathcal{C}$ defined in Section 2.3.
- Computation of the mask $\mathcal{M}$. As markers in $\mathcal{Y}_{\mathrm{mr}}$ often appear smaller than in $\mathcal{Y}_{\mathrm{m}}$ (see Figure 1), the high-intensity regions in $\mathcal{Y}_{\mathrm{mr}}$ are enlarged by morphological dilation [14] with the circle of radius $h/2$ as the structuring element. To have the same intensity for all points within one contiguous region, we group them and assign the largest intensity value to all.
- The mask $\mathcal{M}$ is multiplied with $\mathcal{Y}_{\mathrm{m}}$, and the final MEF-image is produced after another contrast enhancement step with the function $\mathcal{C}$.

Table 1. TPR depending on the kernel size, ℓ, of the Dolph-Chebyshev temporal filter.

ℓ	Quasar	RSVP	Patient 1	Patient 2	Patient 3
1	100	78.17	76.85	92.59	73.15
3	100	95.63	97.22	100	88.89
7	100	99.6	100	100	90.74
11	100	100	100	100	93.52

3. Filter validation

In addition to verifying visually on multiple images that the MEF produces desirable results in terms of marker amplification, background suppression, and marker shape preservation, we have conducted quantitative validation experiments. The fluoroscopic images were acquired at 5.5 Hz at a technique of 120 kVp, 32 mA, 40 ms per frame for phantoms, and 120 kVp, 64 mA, 20 ms for prostate patients. MV irradiation was off.

3.1. MEF success rates

The true positive rate (TPR) is defined as the percentage of the points enhanced by the MEF, i.e., the intensities of which in the MEF-image are higher or equal to τ, that belong to the markers. Table 1 shows median TPR for moving Quasar respiratory phantom (23 frames, linear motion at 2.3 mm/sec), stationary pelvic radio-surgery verification phantom (RSVP, 342 frames), and 3 prostate patients (200 frames each), for images obtained by combining ℓ frames with the Dolph-Chebyshev filter (i.e, temporal filtering). In general, the TPR increases for larger ℓ, and decreases as the region of interest (ROI) grows. Table 1 contains the results for ROIs that measure approximately 45×100 mm (include 7 markers) for the phantoms and 50×70 mm (include 3 markers) for the patients, respectively. Note that substantial TPR improvement is observed from $\ell = 1$ (no temporal filtering) to $\ell = 3$.

3.2. Comparison to other filters

We have also compared the MEF to other filters reported in the literature, such as the MEK [8], LoG^2 [10], Sato's blob filter [12], and Frangi's line filter [11]. The data points in Figure 3 are obtained by computing the median true (TP) and false positives (FP) as a fraction of positives after applying a series of intensity thresholds to 9 filtered sequences, 38 frames each, of the RSVP. As the results suggest, the MEF shows the least FP for high TPs.

4. Discussion

Although it was designed with a particular application in mind, the proposed filter can be used in a variety of marker localization and tracking applications. The main advantages of the MEF over other filters are its marker enhancement and shape preservation properties, and its successful background suppression. No preliminary information about the marker orientation is required. We also observe that the use of temporal filtering prior to the MEF application improves the filtering outcome.

The main limitation of the MEF comes from the assumption that among all features observed at σ_0, the markers should possess the highest contrast. While a couple of features similar to the markers in size and contrast typically do not jeopardize marker localization, especially considering the subsequent registration to the CBCT that is performed in our application, the

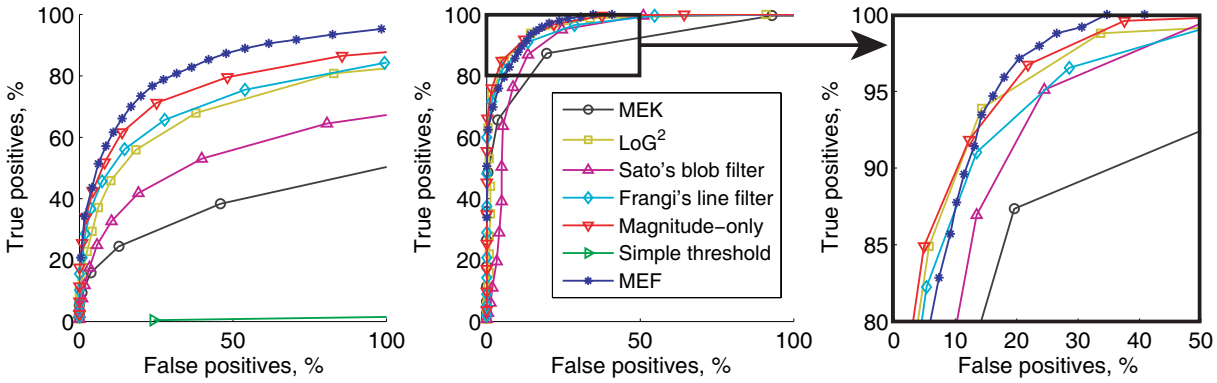

Figure 3. TP and FP rates for different filters for $\ell = 1$ (no temporal filtering, *left*) and $\ell = 7$ (*centre*). The figure on the *right* shows a zoom-in into the high TP and low FP region for $\ell = 7$.

presence of a higher-contrast feature with one of the dimensions corresponding to σ_0 and the other much larger is not desirable.

The scale $\sigma_0 = 0.7$ mm that we have chosen is tuned to the marker diameter. Using a larger scale for $\mathcal{Y}_{\text{mr}}$, i.e., adjusting it to the marker length, may seem a better strategy than the choice to apply morphological dilation, grouping and flattening to produce the mask $\mathcal{M}$. However, we observed that the use of a larger σ_0 for the prostate fluoroscopic images causes an increased filter response in anatomical features that are typically larger than the marker diameter.

Acknowledgments

We would like to thank Dr. Cynthia Menard and Dr. Tim Craig from Princess Margaret Hospital, Toronto, for the patient images provided to test the MEF.

References

[1] Jaffray D A, Siewerdsen J H, Wong J W and Martinez A A 2002 *Int. J. Radiat. Oncol. Biol. Phys.* **53** 1337–49

[2] Moseley D *et al.* 2007 *Int. J. Radiat. Oncol. Biol. Phys.* **67** 942–53

[3] Peshko O, Moseley D J, Craig T, Terlaky T and Menard C 2007 *Med. Phys.* vol 34 p 2392

[4] Peshko O 2013 *Automatic detection and tracking of features in medical images (in preparation)* Ph.D. thesis McMaster University, Hamilton, Canada

[5] Keall P J, Todor A D, Vedam S S, Bartee C L, Siebers J V, Kini V R and Mohan R 2004 *Med. Phys.* **31** 3492–9

[6] Park J C, Park S H, Kim J H, Yoon S M, Kim S S, Kim J S, Liu Z, Watkins T and Song W Y 2011 *Med. Phys.* **38** 1028–36

[7] Mao W, Wiersma R D and Xing L 2008 *Med. Phys.* **35** 1942–49

[8] Nederveen A, Lagendijk J and Hofman P 2000 *Int. J. Radiat. Oncol. Biol. Phys.* **47** 1435–42

[9] Modersitzki J 2004 *Numerical Methods for Image Registration* (New York: Oxford University Press)

[10] Lindeberg T 1994 *Scale-Space Theory in Computer Vision* (Dordrecht: Kluwer Academic Publishers)

[11] Frangi A F, Niessen W J, Vincken K L and Viergever M A 1998 *Medical Image Computing and Computer-Assisted Interventation – MICCAI'98* ed Wells W M *et al.* (Berlin Heidelberg: Springer) pp 130–7

[12] Sato Y, Westin C F, Bhalerao A, Nakajima S, Shiraga N, Tamura S and Kikinis R 2000 *IEEE Trans. Visual. Comput. Graphics* **6** 160–80

[13] Tuytelaars T and Mikolajczyk K 2007 *Foundations and Trends in Computer Graphics and Vision* **3** 177–280

[14] Gonzalez R C, Woods R E and Eddins S L 2004 *Digital Image Processing using Matlab* (Upper Saddle River: Pearson Prentice Hall) pp 334–377

[15] Harris F J 1978 *Proc. IEEE* **66** 51–83

[16] Park S J, Ionascu D, Hacker F, Mamon H and Berbeco R 2009 *Med. Phys.* **36** 4536–46

[17] Buck D, Alber M and Nüsslin F 2003 *Phys. Med. Biol.* **48** 763–74